

Comparison of magnetic field uniformities for discretized and finite-sized standard $\cos \theta$, solenoidal, and spherical coils

N. Nouri, B. Plaster

*Department of Physics and Astronomy, University of Kentucky,
Lexington, Kentucky 40506, USA*

Abstract

A significant challenge for experiments requiring a highly uniform magnetic field concerns the identification and design of a discretized and finite-sized magnetic field coil of minimal size. In this work we compare calculations of the magnetic field uniformities and field gradients for three different standard (i.e., non-optimized) types of coils: $\cos \theta$, solenoidal, and spherical coils. For an experiment with a particular requirement on either the field uniformity or the field gradient, we show that the volume required by a spherical coil form which satisfies these requirements can be significantly less than the volumes required by $\cos \theta$ and solenoidal coil forms.

Keywords: discretized and finite-sized spherical coil, $\cos \theta$ coil, solenoidal coil

1. Introduction

As is well known [1, 2], a solenoid of infinite length will generate a perfectly uniform axial magnetic field everywhere inside of a cylindrical volume. As is also well known [1, 2], an infinitely-long “ $\cos \theta$ coil” (i.e., a cylindrical coil with a continuous surface current $\vec{K} = K \cos \theta \hat{z}$, with the angle θ defined relative to the \hat{y} -axis as shown in Fig. 1), will generate a perfectly uniform transverse magnetic field (along the \hat{x} -direction in Fig. 1) within a cylindrical volume. And indeed, experiments requiring a highly uniform magnetic field have generally employed discretized and finite-length solenoidal or $\cos \theta$ coils for the generation of highly

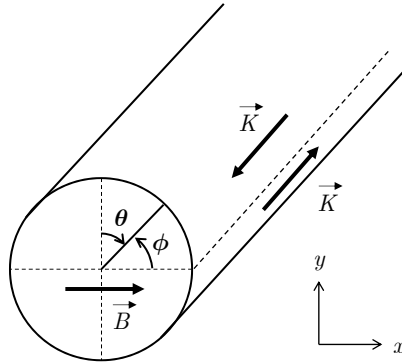


Figure 1: Schematic diagram of a $\cos\theta$ coil with a continuous surface current distribution $\vec{K} = K \cos\theta\hat{z}$. Note that a coil with such a surface current distribution is also commonly referred to as a “sine-phi” coil [3, 4], where the angle ϕ is the usual cylindrical coordinate.

uniform axial or transverse magnetic fields. For example, experimental searches for non-zero permanent electric dipole moments, such as of the neutron and the ^{199}Hg and ^{225}Ra atoms, require highly uniform magnetic fields and past and future experiments [5–10] have typically used highly-optimized $\cos\theta$ or solenoidal coils. In these experiments, the volume required by the $\cos\theta$ and solenoidal cylindrical coil forms is, in general, significantly larger than the sensitive experimental volume over which the requirements on the field uniformity and/or field gradient must be satisfied.

Perhaps less well known or appreciated is the fact that a *finite-sized* spherical coil with a continuous surface current $\vec{K} = K \sin\theta\hat{\phi}$, shown schematically in Fig. 2, where (θ, ϕ) are the usual spherical coordinates, will generate a perfectly uniform magnetic field along the sphere’s \hat{z} -axis within the spherical volume [1–3, 11, 12]. Although the technical challenges associated with the fabrication of an experimentally-realizable discretized spherical coil (e.g., precise wire placement, etc.) may be more significant than those associated with the fabrication of solenoidal and discretized $\cos\theta$ coils, we note that the potential appeal of a spherical coil is that even for the (non-realistic) case of continuous surface currents, a spherical coil of finite size will generate a perfectly uniform field,

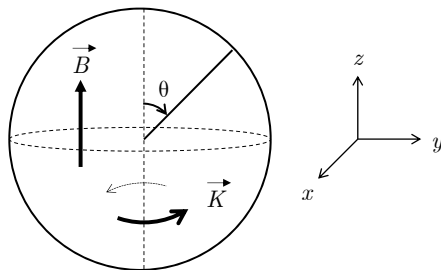


Figure 2: Schematic diagram of a spherical coil with a continuous surface current distribution $\vec{K} = K \sin \theta \hat{\phi}$.

whereas the $\cos \theta$ and solenoidal coils must be of infinite length. That is, a spherical coil does not suffer from any such “finite-length” effects” that are by definition present in finite-sized $\cos \theta$ and solenoidal coils. Therefore, we conjecture that the ratio of the fiducial volume (i.e., the volume over which the requirements on the field uniformity or field gradient must be satisfied) to the total volume occupied by a spherical coil form will be larger than this ratio for $\cos \theta$ and solenoidal coil forms. And, indeed, a new experimental search for the neutron electric dipole moment will employ a spherical coil [13]. However, to our knowledge, detailed calculations of the off-axis field uniformity properties of a discretized spherical coil have not been presented in the literature.

In the remainder of this paper we investigate this conjecture. We begin, in Section 2, by describing our models for our calculations of the magnetic fields for these three coil types, including our methods for the calculation of the off-axis fields for the solenoidal and spherical coils. We then present the numerical results of our calculations in Section 3, where we ultimately compare the ratios of the fiducial volume to the total volume occupied by each of the coil types for various requirements on the field uniformity or field gradient. Finally, we conclude with a summary of our findings in Section 4. We emphasize that throughout this paper we are considering standard (i.e., non-optimized) versions of the $\cos \theta$ and solenoidal coils (i.e., truncated versions of the infinitely-long ideal coils).

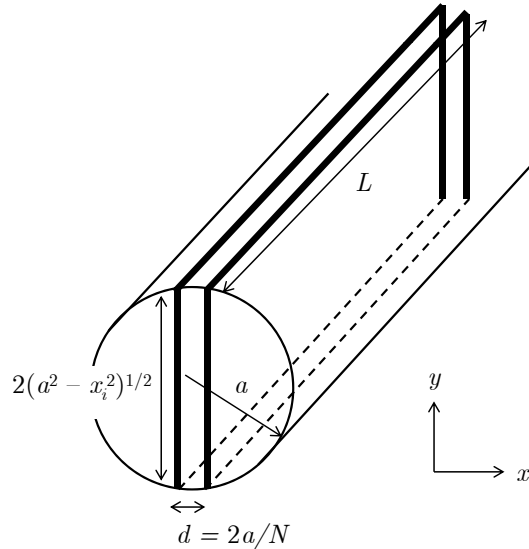


Figure 3: Schematic diagram of our model for a standard discretized and finite-sized $\cos \theta$ coil. The thick lines indicate the rectangular current loops. Note that this choice of a return path for the currents is not unique; another well-known approach is to employ a “saddle-shaped” winding [4, 10], in which the return wires are wound around the perimeters of the cylinder ends.

2. Models for Discretized and Finite-Sized Coils

In this section we describe our numerical models for the calculation of the magnetic fields (on- and off-axis) from discretized and finite-sized $\cos \theta$, solenoidal, and spherical coils. Note that our discretization of the ideal surface currents is such that we use a single point (i.e., zero radius) line wire to approximate regions of equal integrated surface current. We describe our implementation of such for each of the coil types below.

2.1. Model for $\cos \theta$ Coil

A schematic diagram of our discretized and finite-length $\cos \theta$ coil is shown in Fig. 3. As shown in Ref. [4], the discretization of an infinitely-long continuous $\vec{K} = K \cos \theta \hat{z}$ surface current distribution into line currents approximating

the continuous surface current distribution (obtained by apportioning the total integrated current from $\theta = 0$ to $\pi/2$ into equal discrete parts) is such that the line currents are spaced at equal intervals along the indicated x -axis. Thus, as indicated in Fig. 3, our model consists of a cylindrical shell of radius a and length L , upon which are wound N rectangular current loops, spaced at equal intervals $d = 2a/N$ along the x -axis at positions $x = \pm\frac{1}{2}d, \pm\frac{3}{2}d, \dots, \pm\frac{N-1}{2}d$. The line currents then flow in the $+z$ ($-z$) direction for $\cos\theta > 0$ (< 0) along the length of the cylinder. Our model then assumes a simple return path for the currents (i.e., straight line currents along the $\pm y$ direction), such that our closed current loops are rectangular. Thus, all of the rectangular current loops are of the same length L along the axis of the cylindrical form (i.e., the z -axis), but are of different lengths along the y -axis, where these lengths are constrained by the cylindrical form to be $2\sqrt{a^2 - x_i^2}$, where x_i denotes the i th loop's position along the x -axis.

The calculations we present later have assumed N even; one could, of course, consider N odd, with an additional wire located at $\theta = 0$, but this would not modify the symmetry of the problem. Also, note that although our model does not include any connecting wires between adjacent current loops (which are, of course, required if a $\cos\theta$ is to be wound with a single wire), an actual $\cos\theta$ coil can be wound in such a way so that the contributions to the field from the connecting wires carrying the current from, say, loop i to loop $i+1$ to loop $i+2$, etc. are largely cancelled by the return wire to the current source.

It is then straightforward to calculate the magnetic field everywhere in space in rectangular coordinates via the Biot-Savart law.

2.2. Model for Solenoidal Coil

Because the surface current distribution on an ideal solenoid is uniform in the cylindrical coordinates ϕ and z (with z oriented the solenoid axis), such that $\vec{K} = K\hat{\phi}$, our model for a discretized and finite-length solenoidal coil consists of a cylindrical coil form of radius a and length L upon which are wound N circular current loops of radius a oriented in the indicated xy -plane and spaced

at equal intervals d along the length of the cylinder. Note that each of our discretized current loops is “isolated” (i.e., stand-alone circular loops, with no connecting wires), such that we do not attempt to account for the effects of a helical winding inherent to the winding of a solenoid with one continuous wire.

We then employ cylindrical coordinates to calculate the magnetic field of our solenoidal coil at some observation point $\vec{x} = (\rho, \phi, z)$. By symmetry, the vector potential $\vec{A}_i(\vec{x})$ of the i th circular current loop centered at $(0, 0, z_i)$ includes only a ϕ -component, and is of the form [1, 2]

$$A_{\phi,i}(\rho, z) = \frac{\mu_0 I}{\pi \kappa_i} \sqrt{\frac{a}{\rho}} \left[\left(1 - \frac{1}{2} \kappa_i^2 \right) K(\kappa_i) - E(\kappa_i) \right], \quad (1)$$

where $K(\kappa_i)$ and $E(\kappa_i)$ denote, respectively, the complete elliptic integrals of the first and second kind, $\kappa_i^2 \equiv 4a\rho/[(a+\rho)^2 + (\Delta z_i)^2]$, and $\Delta z_i \equiv z - z_i$.

The resulting ρ - and z -components of the $\vec{B}_i(\vec{x})$ field at \vec{x} due to the i th circular current loop are then calculated as $\vec{B} = \vec{\nabla} \times \vec{A}$ in cylindrical coordinates and are of the form

$$\begin{aligned} B_{\rho,i}(\vec{x}) &= \frac{\mu_0 I (\Delta z_i)}{2\pi \rho \sqrt{(a+\rho)^2 + (\Delta z_i)^2}} \left[-K(\kappa_i) + \frac{a^2 + \rho^2 + (\Delta z_i)^2}{(a-\rho)^2 + (\Delta z_i)^2} E(\kappa_i) \right], \\ B_{z,i}(\vec{x}) &= \frac{\mu_0 I}{2\pi \sqrt{(a+\rho)^2 + (\Delta z_i)^2}} \left[K(\kappa_i) + \frac{a^2 - \rho^2 - (\Delta z_i)^2}{(a-\rho)^2 + (\Delta z_i)^2} E(\kappa_i) \right], \end{aligned} \quad (2)$$

with the complete elliptic integrals then expressed as power series [14] in the parameter κ_i ,

$$\begin{aligned} K(\kappa_i) &= \frac{\pi}{2} \left\{ 1 + \sum_{n=1}^{\infty} \left[\frac{(2n-1)!!}{(2n)!!} \right]^2 \kappa_i^{2n} \right\}, \\ E(\kappa_i) &= \frac{\pi}{2} \left\{ 1 - \sum_{n=1}^{\infty} \left[\frac{(2n-1)!!}{(2n)!!} \right]^2 \frac{\kappa_i^{2n}}{2n-1} \right\}. \end{aligned} \quad (3)$$

Note that the values of κ_i are restricted to the range $0 \leq \kappa_i \leq 1$. We sum the power series until the contribution of the n th term is $< 10^{-9}$. The resulting $B_{\rho,i}(\vec{x})$ and $B_{z,i}(\vec{x})$ field components for each circular current loop are then converted to rectangular field components. The total field $\vec{B}(\vec{x})$ at observation

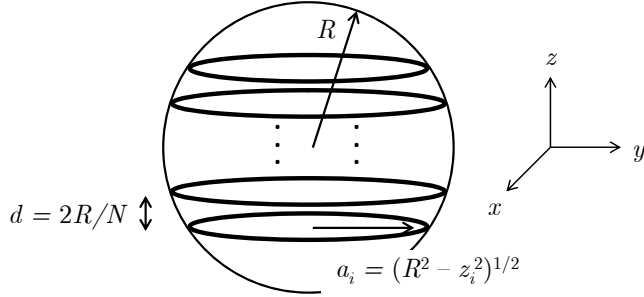


Figure 4: Schematic diagram of our model for a standard discretized spherical coil. The thick lines indicate the circular current loops.

point \vec{x} from all N circular current loops comprising the discretized solenoidal coil is then simply the superposition of the rectangular field components from each of the current loops.

2.3. Model for Spherical Coil

Finally, a schematic diagram of our discretized spherical coil is shown in Fig. 4. As indicated there, our model consists of a spherical form of radius R upon which are wound N circular current loops oriented in the xy -plane. The discretization of the spherical coil's $\vec{K} = K \sin \theta \hat{\phi}$ continuous surface current distribution into N discrete line wires proceeds in an identical manner to how the discretization of a $\cos \theta$ coil current is performed in Ref. [4], and is as follows. Suppose we desire to divide the integral of the surface current, $\propto \int_0^\pi \sin \theta R d\theta \propto 2R$, into N equal parts, with each part bounded by the angles $[\alpha_{i-1}, \alpha_i]$ for $i = 1, 2, \dots, N$, where $\alpha_0 = 0$ and $\alpha_N = \pi$. We then approximate each of these parts carrying equal currents $\propto 2R/N$ with a wire. Then, let θ_i denote the angular position of the i th wire, where θ_i locates the midpoint of the integrated surface current over the angular interval $[\alpha_{i-1}, \alpha_i]$. Thus, per these definitions, θ_i must satisfy the condition

$$\int_{\alpha_{i-1}}^{\theta_i} \sin \theta R d\theta = \int_{\theta_i}^{\alpha_i} \sin \theta R d\theta = \frac{1}{2} \frac{2R}{N}. \quad (4)$$

From this, it follows that $\cos \alpha_{i-1} - \cos \alpha_i = 2/N$, and so starting from $\alpha_0 = 0$, we find that $\cos \alpha_i = 1 - 2i/N$. From the above integrals, it also follows that $\cos \theta_i = \cos \alpha_{i-1} - 1/N$, from which it then follows that the z -coordinate for the i th discretized wire is

$$z_i = R \cos \theta_i = R \left(1 - \frac{2i-1}{N} \right). \quad (5)$$

This shows that a discretized approximation to a spherical coil consists of circular current loops spaced at equal intervals of $d = 2R/N$ along the z -axis at positions $z_i = \pm \frac{1}{2}d, \pm \frac{3}{2}d, \dots, \pm \frac{N-1}{2}d$. From this, it then follows that the radius a_i of the i th current loop is constrained to be $a_i = \sqrt{R^2 - z_i^2}$, and the radii of the two smallest loops, at positions $z_1 = -z_N = \frac{N-1}{2}d$, are $a_1 = a_N = \sqrt{R^2 - z_{1,N}^2}$. Again, we note that the above is for N even; however, as before, N odd, with a wire at $\theta = \pi/2$, would not modify the symmetry of the problem.

To calculate the magnetic field of our discretized spherical coil everywhere inside of the coil, we now employ (r, θ, ϕ) spherical coordinates, where the origin is located at the center of our spherical coil. As shown in Refs. [2, 15], the vector potential $A_{\phi,i}(\vec{x})$ of the i th circular current loop (located at $\theta = \theta_i$) at some observation point $\vec{x} = (r < R, \theta, \phi)$, as derived via the stream function approach, is of the form

$$A_{\phi,i}(\vec{x}) = \frac{\mu_0 I}{2} \sum_{n=1}^{\infty} \frac{\sin \theta_i}{n(n+1)} \left(\frac{r}{R} \right)^n P_n^1(\cos \theta_i) P_n^1(\cos \theta). \quad (6)$$

From this, it then follows that the r_i - and θ_i -components of the magnetic field at \vec{x} , as calculated from $\vec{B} = \vec{\nabla} \times \vec{A}$ in spherical coordinates, are then for $r < R$ of the explicit form

$$\left. \begin{array}{l} B_{r,i}(\vec{x}) \\ B_{\theta,i}(\vec{x}) \end{array} \right\} = \frac{\mu_0 I \sin \theta_i}{2R} \sum_{n=1}^{\infty} \left(\frac{r}{R} \right)^{n-1} P_n^1(\cos \theta_i) \left\{ \begin{array}{l} P_n(\cos \theta) \\ -\frac{1}{n} P_n^1(\cos \theta) \end{array} \right\}, \quad (7)$$

where P_n denotes the ordinary Legendre polynomial and P_n^1 the associated Legendre polynomial. We then summed the field components from all of the current loops comprising the spherical coil, and then converted the resulting $B_r(\vec{x})$ and $B_\theta(\vec{x})$ field components in spherical coordinates to rectangular field components, ultimately for comparison with the other two coil types.

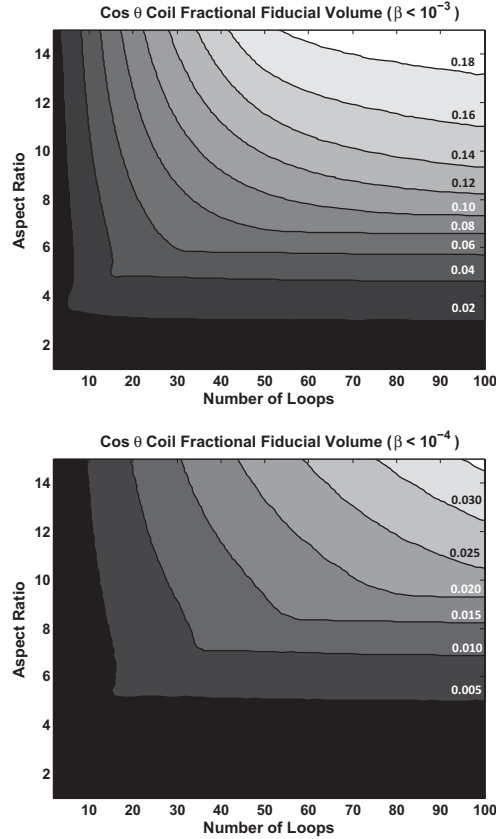


Figure 5: Fractional fiducial volume for $\beta < 10^{-3}$ (top plot) and $< 10^{-4}$ (bottom plot) field uniformities for a standard discretized and finite-sized $\cos\theta$ coil, as a function of the number of rectangular loops and the coil’s aspect ratio, or length-to-radius ratio L/a .

3. Comparisons of Field Uniformities and Field Gradients

We now compare the field uniformities and gradients from standard discretized and finite-sized $\cos\theta$, solenoidal, and spherical coils for two example scenarios. First, to illustrate the fiducial volume properties of these coils, we show in Figs. 5–7 calculations of each coil’s fractional fiducial volume (i.e., the fraction of each coil’s volume which satisfies the fiducial volume requirement) for 10^{-3} and 10^{-4} field uniformities, where we define the field uniformity β at

some point \vec{x} relative to the center of the coil, $\vec{x} = 0$, to be

$$\beta \equiv \left| \frac{|\vec{B}(\vec{x})| - |\vec{B}(\vec{x} = 0)|}{|\vec{B}(\vec{x} = 0)|} \right|. \quad (8)$$

The calculations for the $\cos \theta$ coil are shown in Fig. 5 for $\beta < 10^{-3}$ and $< 10^{-4}$ in two-dimensional parameter space of the number of rectangular current loops, N , and the coil's length-to-radius ratio, L/a . Those for the solenoidal coil are shown in Fig. 6 for $\beta < 10^{-3}$ and $< 10^{-4}$ in two-dimensional parameter space in terms of the number of circular loops, and the solenoid's length-to-radius ratio, L/a . Finally, those for the spherical coil are shown in Fig. 7 for $\beta < 10^{-3}$ and $< 10^{-4}$ as a function of the number of turns, which is the only free parameter for a standard spherical coil of fixed radius.

We note that for the $\cos \theta$ and solenoidal coils, further increases in the number of turns N beyond the upper range of $N = 100$ shown in Figs. 5–6 does not lead to appreciable increases in their fractional fiducial volumes. Thus, our results clearly indicate that the fractional fiducial volume of a spherical coil can be significantly larger (by up to an order of magnitude for spherical coils consisting of > 60 circular loops) than those of $\cos \theta$ and solenoidal coils. As a visual illustration of the uniformity properties of a spherical coil, Fig. 8 shows the fiducial volumes of 1.0-m radius spherical coils consisting of $N = 10, 30$, and 50 circular loops which satisfy a $\beta < 10^{-3}$ and $< 10^{-4}$ field uniformity requirement.

As a second example, we consider an experimental requirement on the fractional field gradient, γ , which we define to be

$$\gamma \equiv \frac{1}{|\vec{B}(\vec{x} = 0)|} \left| \frac{\partial B_i}{\partial x_i} \right|, \quad (9)$$

where B_i denotes the field component along the field's primary direction (i.e., the x -component for the $\cos \theta$ coil and the z -component for the solenoidal and spherical coils). To illustrate, suppose a hypothetical requirement is that $\gamma < 10^{-5}$ everywhere inside of a $10 \times 10 \times 10 \text{ cm}^3$ rectangular volume located at the center of each coil. In Table 1 we show examples of spherical coil geometry parameters

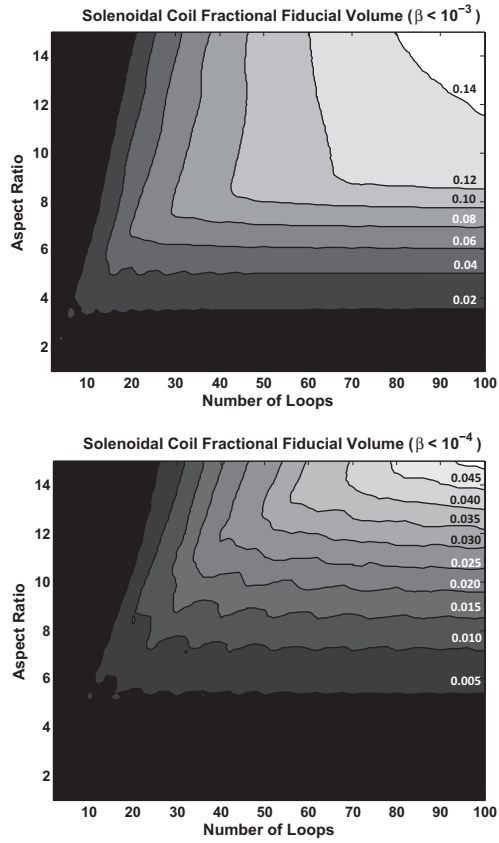


Figure 6: Fractional fiducial volume for $\beta < 10^{-3}$ (top plot) and $\beta < 10^{-4}$ (bottom plot) field uniformities for a standard discretized and finite-sized solenoidal coil, as a function of the number of circular loops comprising the solenoid and the coil's aspect ratio, or length-to-radius ratio L/a .

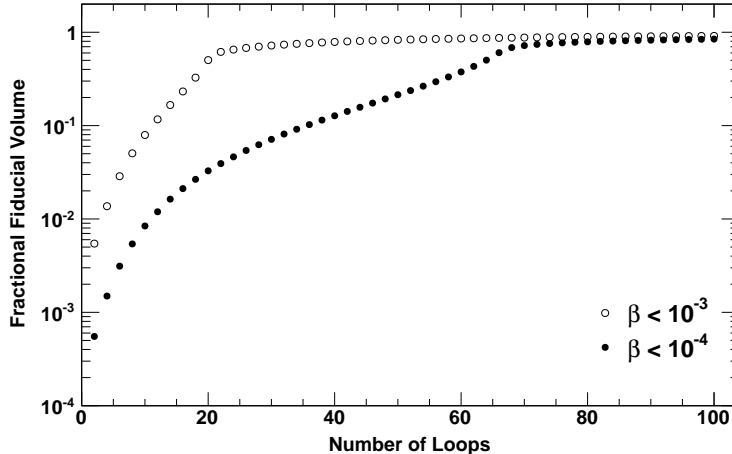


Figure 7: Fractional fiducial volume for $\beta < 10^{-3}$ (open circles) and $\beta < 10^{-4}$ (filled circles) field uniformities for a standard discretized spherical coil, as a function of the number of circular loops comprising the spherical coil.

which would satisfy this requirement, and compare these with benchmark examples of geometry parameters for approximate best-case $\cos \theta$ and solenoidal coils (i.e., large length-to-radius ratios and number of turns, as suggested by the fractional fiducial volume calculations presented in Figs. 5–6). Our results indicate that a particular requirement on the fractional field gradient could be achieved with a spherical coil occupying a smaller volume than the volumes occupied by $\cos \theta$ and solenoidal coils.

However, we do note that a potential appeal of the $\cos \theta$ -coil (if wound with a “saddle winding” [4, 10]) and solenoidal-coil geometries is that their winding patterns permit significant access to their interior regions along their respective z -axes (i.e., via a circular aperture of radius equal to the radius a of their cylindrical form), whereas access to the interior of a spherical coil along its z -axis is constrained by the radii of the two smallest current loops, $a_1 = a_N = \sqrt{R^2 - z_{1,N}^2}$, located at positions $z_1 = -z_N = \frac{N-1}{2}d$, as discussed previously in Section 2.3. If a $\cos \theta$ coil is wound with rectangular loops (as in

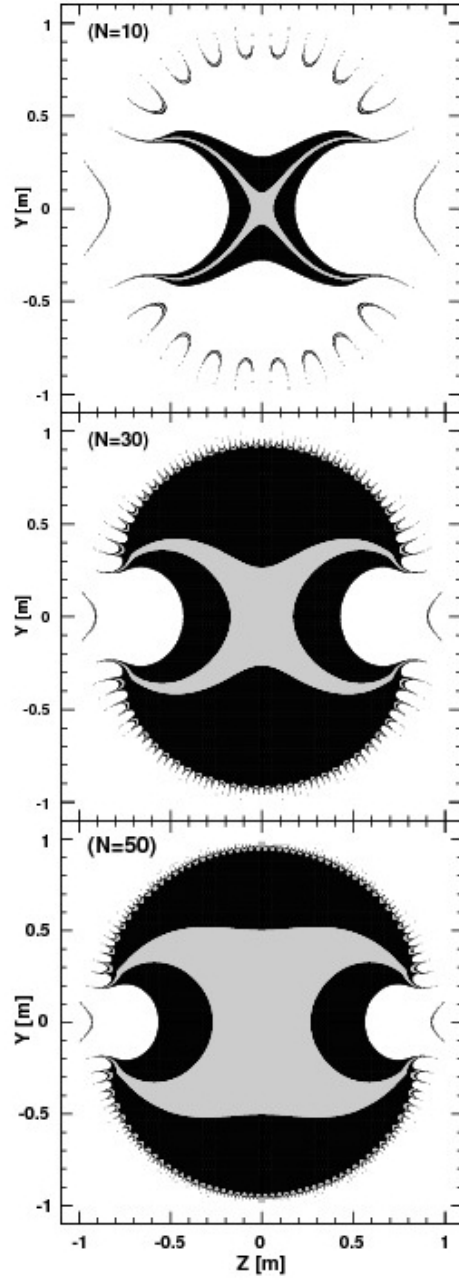


Figure 8: Visualization of the fractional fiducial volumes of 1.0-m radius spherical coils consisting of $N = 10, 30,$ and 50 circular loops which satisfy $\beta < 10^{-3}$ (dark regions) and $< 10^{-4}$ (gray regions) field uniformities. Note that the circular current loops are in the xy plane.

Table 1: Geometry parameters for spherical coils (number of turns N , radius of sphere R , and the resulting radii of the two smallest current loops $a_{\min} \equiv a_1 = a_N$; see text in Section 2.3) which would satisfy a requirement on the fractional field gradient of $\gamma < 10^{-5}$ everywhere inside of a $10 \times 10 \times 10 \text{ cm}^3$ cube. These are compared with geometry parameters (number of turns N , radius of cylindrical coil form a , and length of cylindrical coil form L) for benchmark $\cos \theta$ and solenoidal coils. The total volume V occupied by each coil form is also listed.

Coil	N	R [cm]	a_{\min} [cm]	V [m ³]
Spherical	20	87	27.2	2.76
Spherical	40	45	10.0	0.38
Spherical	60	31	5.64	0.12
Spherical	80	24	3.78	0.06
Spherical	100	20	2.82	0.03
Coil	N	a [cm]	L [cm]	V [m ³]
$\cos \theta$	100	19	229	0.26
Solenoidal	100	13	249	0.13

our model calculations), access to the interior along its z -axis is restricted by the spacing $d = 2a/N$ between adjacent rectangular loops (see Fig. 3).

For access to their interior regions along the transverse direction, the dimensions of the $\cos \theta$ coil’s two smallest rectangular loops are $\frac{2a}{N} \sqrt{2N-1}$ (y -direction) $\times L$ (z -direction; see Fig. 3). The solenoidal coil can, in principle, be accessed in the transverse direction via the gaps of size $\frac{L}{N-1}$ in between adjacent circular windings, and the spherical coil can also be accessed in the transverse direction in between the circular current loops, which are spaced at equal intervals of $d = 2R/N$ along its z -axis (see Fig. 4).

4. Summary

In this paper we have presented a model for numerical calculations of the magnetic field of a standard discretized spherical coil. Because a discretized spherical coil does not suffer from any “finite-length effects” that are inherent

to standard discretized and finite-sized $\cos\theta$ and solenoidal coils, our calculations indicate that the fractional fiducial volume of a discretized spherical coil is potentially significantly larger than those of standard (i.e., non-optimized) discretized and finite-length $\cos\theta$ and solenoidal coils.

Acknowledgments

This work was supported in part by the U. S. Department of Energy Office of Nuclear Physics under Award Number DE-FG02-08ER41557. We thank Prof. J. W. Martin for encouraging us to write this paper, and Prof. C. B. Crawford for several valuable discussions. We also thank an anonymous referee for many excellent suggestions which, we believe, significantly improved this paper.

References

- [1] J. D. Jackson, *Classical Electrodynamics*, Third Edition (John Wiley & Sons, Inc., 1999). See Problems 5.2 (solenoid), 5.13 (sphere), and 5.30 ($\cos\theta$). See pp. 181–184 for a discussion of the vector potential \vec{A} of a circular current loop.
- [2] W. R. Smythe, *Static and Dynamic Electricity*, Third Edition, Revised Printing (Taylor & Francis, 1989). See pp. 290–299.
- [3] J.-M. Jin, IEEE Antennas and Propagation Magazine **40**, 7 (1998).
- [4] C. P. Bidinosti, I. S. Kravchuk, and M. E. Hayden, J. Magn. Reson. **177**, 31 (2005).
- [5] C. A. Baker *et al.*, Phys. Rev. Lett. **97**, 131801 (2006).
- [6] S. N. Balashov *et al.*, [arXiv:0709.2428](https://arxiv.org/abs/0709.2428) .
- [7] I. Altarev *et al.*, Nucl. Instrum. Methods Phys. Res. A **611**, 133 (2009).

- [8] W. C. Griffith *et al.*, Phys. Rev. Lett. **102**, 101601 (2009).
- [9] R. J. Holt *et al.*, Nucl. Phys. A **844**, 53c (2010).
- [10] A. Pérez Galván *et al.*, Nucl. Instrum. Methods Phys. Res. A **660**, 147 (2011).
- [11] J. E. Everett and J. E. Osemeikhian, J. Sci. Instrum. **43**, 470 (1966).
- [12] H. A. Haus and J. R. Melcher, *Electromagnetic Fields and Energy* (Prentice-Hall, 1989). See Section 8.5.
- [13] Y. Masuda *et al.*, Phys. Lett. A **376**, 1347 (2012).
- [14] G. B. Arfken and H. J. Weber, *Mathematical Methods for Physicists*, Sixth Edition (Elsevier Academic Press, 2005). See pp. 370–374.
- [15] V. C. A. Ferraro, *Electromagnetic Theory*, Fifth Impression (Athlone Press, London, 1954). See pp. 317, 413–424.